AGU PUBLICATIONS

JGR

Journal of Geophysical Research: Atmospheres

RESEARCH ARTICLE
10.1002/2015JD024687

Key Points:
- Atmospheric circulation response to increased CO_2 does not always correlate with climate sensitivity
- Northern Hemisphere circulation response is very poorly correlated with climate sensitivity
- Southern Hemisphere circulation response is also correlated with surface temperature gradients

Correspondence to:
K. M. Grise,
kmg3r@virginia.edu

Citation:
Grise, K. M., and L. M. Polvani (2016), Is climate sensitivity related to dynamical sensitivity?, *J. Geophys. Res. Atmos.*, *121*, 5159–5176, doi:10.1002/2015JD024687.

Received 19 DEC 2015
Accepted 25 APR 2016
Accepted article online 28 APR 2016
Published online 17 MAY 2016

Is climate sensitivity related to dynamical sensitivity?

Kevin M. Grise[1] and Lorenzo M. Polvani[2]

[1]Department of Environmental Sciences, University of Virginia, Charlottesville, Virginia, USA, [2]Department of Applied Physics and Applied Mathematics, Department of Earth and Environmental Sciences, and Lamont-Doherty Earth Observatory, Columbia University, New York, New York, USA

Abstract The atmospheric response to increasing CO_2 concentrations is often described in terms of the equilibrium climate sensitivity (ECS). Yet the response to CO_2 forcing in global climate models is not limited to an increase in global-mean surface temperature: for example, the midlatitude jets shift poleward, the Hadley circulation expands, and the subtropical dry zones are altered. These changes, which are referred to here as "dynamical sensitivity," may be more important in practice than the global-mean surface temperature. This study examines to what degree the intermodel spread in the dynamical sensitivity of 23 Coupled Model Intercomparison Project phase 5 (CMIP5) models is captured by ECS. In the Southern Hemisphere, intermodel differences in the value of ECS explain ~60% of the intermodel variance in the annual-mean Hadley cell expansion but just ~20% of the variance in the annual-mean midlatitude jet response. In the Northern Hemisphere, models with larger values of ECS significantly expand the Hadley circulation more during winter months but contract the Hadley circulation more during summer months. Intermodel differences in ECS provide little significant information about the behavior of the Northern Hemisphere subtropical dry zones or midlatitude jets. The components of dynamical sensitivity correlated with ECS appear to be driven largely by increasing sea surface temperatures, whereas the components of dynamical sensitivity independent of ECS are related in part to changes in surface temperature gradients. These results suggest that efforts to narrow the spread in dynamical sensitivity across global climate models must also consider factors that are independent of global-mean surface temperature.

1. Introduction

Global climate models indicate that the atmospheric circulation will respond to increasing carbon dioxide (CO_2) concentrations in several characteristic ways (see also recent reviews by *Schneider et al.* [2010] and *Vallis et al.* [2015]). In the tropics, the Hadley circulation is projected to weaken [*Held and Soden*, 2006; *Vecchi and Soden*, 2007; *Kang et al.*, 2013] and widen [*Lu et al.*, 2007; *Frierson et al.*, 2007; *Lu et al.*, 2008; *Hu et al.*, 2013], and the subtropical dry zones are projected to shift poleward [*Lu et al.*, 2007; *Johanson and Fu*, 2009; *Scheff and Frierson*, 2012]. In the extratropics, the midlatitude jet stream is projected to shift poleward in both hemispheres, with the most prominent shift occurring in the Southern Hemisphere (SH) [*Kushner et al.*, 2001; *Yin*, 2005; *Miller et al.*, 2006; *Swart and Fyfe*, 2012; *Barnes and Polvani*, 2013; *Simpson et al.*, 2014]. Additionally, as the jets move poleward, their dominant modes of internal variability are projected to change, and the SH jet is projected to increase in speed [*Barnes and Polvani*, 2013].

While global climate models are generally in agreement about the pattern of the atmospheric circulation response to increased CO_2 concentrations, the magnitude of the response varies widely across different models. One might be tempted to naively assume that the intermodel spread in the magnitude of the atmospheric circulation response to increased CO_2 (which we term "dynamical sensitivity") is closely tied to the intermodel spread in the magnitude of the global-mean surface temperature response (i.e., the equilibrium climate sensitivity or ECS). For instance, for a given increase in atmospheric CO_2 concentrations, a model with a greater global-mean surface temperature warming might be expected to shift the midlatitude jet further poleward. However, in a recent paper [*Grise and Polvani*, 2014a, hereafter GP14], we demonstrated that this is not always the case, at least in the SH. Although the magnitude of the poleward expansion of the SH Hadley circulation was found to be significantly correlated with ECS during all seasons, the poleward shifts of the SH midlatitude jet and subtropical dry zones were only found to be significantly correlated with ECS during summer and fall. Additionally, *Vallis et al.* [2015] found little evidence for correlations between the magnitudes of the transient responses of the surface wind field and global-mean surface temperature to increasing CO_2.

Numerous mechanisms have been proposed to explain the dynamical sensitivity of global climate models, some of which have a direct link to global-mean surface temperature and others of which do not. For example, the slowdown of the Hadley circulation has been linked to lower tropospheric water vapor increases, which are directly related to the global-mean surface temperature response via the Clausius-Clapeyron relationship [*Held and Soden*, 2006]. Additionally, the poleward expansion of the Hadley circulation and the poleward shifts in the midlatitude jets have been linked to the moist adiabatic adjustment of tropospheric lapse rates to surface warming, hence increasing the static stability of the subtropics and midlatitudes and suppressing baroclinic eddy growth on the equatorward flanks of the jets [*Frierson et al.*, 2007; *Lu et al.*, 2010; *Kang and Lu*, 2012]. The moist adiabatic adjustment of tropical tropospheric lapse rates also contributes to an enhanced pole-to-equator temperature gradient in the upper troposphere-lower stratosphere, which could lead to a poleward shift of the midlatitude jets [*Butler et al.*, 2010; *Arblaster et al.*, 2011; *Wilcox et al.*, 2012; *Harvey et al.*, 2014; *Gerber and Son*, 2014].

Other proposed mechanisms for dynamical sensitivity are not as directly linked with global-mean surface temperature. For example, changes to the surface temperature gradient could produce notable changes in the position of the midlatitude jet [*Brayshaw et al.*, 2008; *Ring and Plumb*, 2008; *Chen et al.*, 2010]. Using an idealized model, *Butler et al.* [2010] demonstrated that enhanced localized warming of the Arctic surface weakens the surface pole-to-equator temperature gradient and acts to shift the Northern Hemisphere (NH) midlatitude jet equatorward. Likewise, *Ceppi et al.* [2012] suggested that variations in surface temperature gradients can be driven by biases in model cloud-radiative properties, and thus, variations in model cloud parameterizations could influence the magnitude of the SH midlatitude jet's response to increased CO_2 [*Ceppi et al.*, 2014]. Additional mechanisms proposed to explain the midlatitude jet shifts include rises in tropopause height [*Lorenz and DeWeaver*, 2007], increases in the phase speed of baroclinic eddies [*Chen and Held*, 2007; *Chen et al.*, 2008], increases in the length scale of baroclinic eddies [*Kidston et al.*, 2010; *Kidston et al.*, 2011], increased wave reflection on the poleward flank of the jet [*Lorenz*, 2014], and biases in the climatological positions of the jets [*Kidston and Gerber*, 2010; *Barnes and Hartmann*, 2010; GP14].

In this paper, we revisit the processes responsible for the intermodel spread in dynamical sensitivity for the latest generation of global climate models, those that participated in the Coupled Model Intercomparison Project phase 5 (CMIP5). Specifically, we ask which components of dynamical sensitivity can be directly explained by the global-mean surface temperature response (i.e., the ECS) and which components are independent of ECS. Here we focus on the long-term responses of the atmospheric circulation and global-mean surface temperature as they approach a steady state, equilibrated climate with elevated CO_2 concentrations. We have also examined the correlations between the transient responses of the atmospheric circulation and global-mean surface temperature (the so-called transient climate response or TCR) and found the results to be qualitatively similar to those documented here.

In particular, we focus on three metrics of dynamical sensitivity: the latitude of the midlatitude eddy-driven jets, the poleward edges of the subtropical dry zones, and the poleward edges of the Hadley circulation. For each metric, we identify the component of its response to increased CO_2 that is correlated with ECS, thereby extending the SH analysis of GP14 to the global circulation. This component of the response captures common dynamical mechanisms shared collectively across CMIP5 models that are directly related to global-mean surface temperature. The remainder of the response, which by definition is independent of ECS, then can be used to explore additional physical mechanisms (unrelated to ECS) that are responsible for intermodel spread in dynamical sensitivity across global climate models.

The paper is organized as follows. Section 2 describes the data and methods used in this study. Section 3 documents the correlations between our three metrics of dynamical sensitivity and ECS. Section 4 then puts these results into broader context, by examining the role of ECS in the entire zonal-mean global circulation response to increased CO_2. Section 5 provides a discussion of potential physical mechanisms responsible for the intermodel spread in dynamical sensitivity. Section 6 concludes with summarizing thoughts.

2. Data and Methods

The primary data used in this study are the output from 23 of the global climate models that participated in CMIP5 [*Taylor et al.*, 2012]. The data are obtained from the Program for Climate Model Diagnosis and

Table 1. Listing of the CMIP5 Models Used in This Study[a]

	Model	2× Equilibrium Climate Sensitivity (K)	Global-Mean Surface Temperature Response (K)
1	ACCESS1-0	7.66	5.48
2	bcc-csm1-1	5.64	4.81
3	bcc-csm1-1-m	5.74	4.98
4	CanESM2	7.38	5.89
5	CCSM4	5.78	4.78
6	CNRM-CM5	6.50	5.15
7	CSIRO-Mk3-6-0	8.16	5.53
8	FGOALS-s2	8.34	5.84
9	GFDL-CM3	7.94	5.60
10	GFDL-ESM2G	4.78	3.78
11	GFDL-ESM2M	4.88	3.79
12	GISS-E2-H	4.62	4.02
13	GISS-E2-R	4.22	3.39
14	HadGEM2-ES	9.18	6.22
15	inmcm4	4.16	3.01
16	IPSL-CM5A-LR	8.26	5.72
17	IPSL-CM5B-LR	5.22	4.15
18	MIROC5	5.44	4.14
19	MIROC-ESM	9.34	6.42
20	MPI-ESM-LR	7.26	5.87
21	MPI-ESM-P	6.90	5.71
22	MRI-CGCM3	5.20	4.32
23	NorESM1-M	5.60	4.14

[a](middle column) Twice the equilibrium climate sensitivities, reproduced from *Forster et al.* [2013]. (right column) Global-mean surface temperature response, calculated as the difference between each model's preindustrial control run and the last 50 years of each model's 150 year abrupt 4×CO_2 run.

Intercomparison at Lawrence Livermore National Laboratory. The selected models are those with values of ECS defined in *Forster et al.* [2013] (see Table 1).

For each of the models in Table 1, we analyze two different forcing scenarios: (1) preindustrial control (i.e., hundreds of years of unforced variability) and (2) abrupt 4×CO_2 (in which atmospheric CO_2 is instantaneously quadrupled at the beginning of a 150 year run). For each scenario, we use the first ensemble member ("r1i1p1") from each model. We calculate the preindustrial control climatology of each model using the average of all available years from the preindustrial control run, and we calculate the 4×CO_2 climatology of each model using the average of the last 50 years from the abrupt 4×CO_2 run. The last 50 years of the abrupt 4×CO_2 run are taken as the best available estimate of the equilibrated 4×CO_2 climate, as the global-mean surface temperature response over this period is correlated with ECS at $r = 0.95$ (compare second and third columns in Table 1). Note that, because ECS has been traditionally defined with respect to a doubling of CO_2, we have multiplied the values of ECS from *Forster et al.* [2013] by two throughout this paper, such that our values correspond to a 4×CO_2 climate.

Following GP14, we define dynamical sensitivity using three metrics. The three metrics are illustrated in Figure 1, which shows the observed climatology of the annual-mean, zonal-mean circulation from the ERA-Interim reanalysis [*Dee et al.*, 2011].

The metrics are defined as follows:

1. *Latitude of the midlatitude eddy-driven jet* (ϕ_{u850}). We define ϕ_{u850} in each hemisphere as the latitude where the zonal-mean, zonal wind field (Figure 1, thick blue lines) reaches its peak value at 850 hPa.
2. *Poleward edge of the subtropical dry zone* ($\phi_{P-E=0}$). We define $\phi_{P-E=0}$ in each hemisphere as the latitude where the zonal-mean precipitation minus evaporation crosses zero poleward of its subtropical minimum (Figure 1, brown zones).
3. *Poleward boundary of the Hadley circulation* ($\phi_{\Psi 500}$). We define $\phi_{\Psi 500}$ as the latitude where the 500 hPa mean meridional mass stream function (Figure 1, thin red lines) crosses zero poleward of its tropical maximum in the NH and its tropical minimum in the SH.

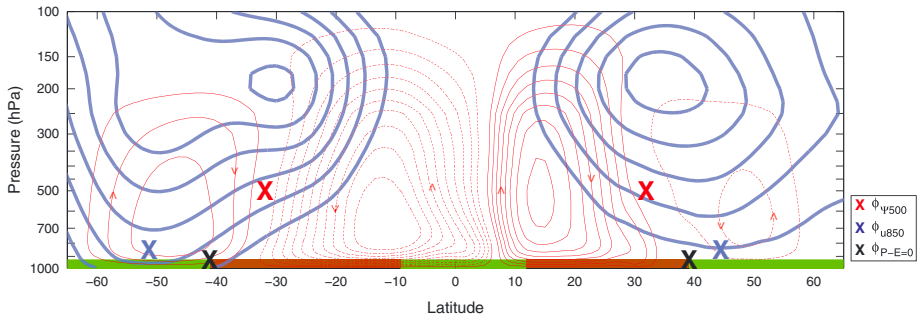

Figure 1. Annual-mean, zonal-mean 1979–2012 ERA-Interim reanalysis climatology. Thick blue lines denote the zonal-mean zonal wind (contour interval: 5 m s^{-1}, for values ≥5 m s^{-1}), and thin red lines denote the mean meridional mass stream function (contour interval: 1.0×10^{10} kg s^{-1}; negative contours dashed and zero contour omitted). Regions where zonal-mean precipitation is greater (less) than zonal-mean evaporation are shaded in green (brown).

For each metric, a polynomial fit to the model data is used to find the appropriate latitude at a resolution of 0.01° [see also *Barnes and Polvani*, 2013].

Figure 2 illustrates the seasonal cycle of the three metrics, within the context of the zonal-mean circulation. Results are shown for both the observed and multimodel mean climatologies. In both hemispheres, the winter branch of the Hadley circulation (thin solid lines in NH and thin dashed lines in SH) is stronger, and $\phi_{\Psi 500}$ is further equatorward during winter months. During summer months, the Hadley circulation weakens significantly, and $\phi_{\Psi 500}$ shifts poleward by ~8° in the SH and ~14° in the NH. In contrast, the 850 hPa midlatitude jet is more sharply defined during December–February in both hemispheres. ϕ_{u850} has little seasonality in the SH but is further equatorward in winter in the NH by ~11°. The seasonal cycle of $\phi_{P-E=0}$ in both hemispheres generally mirrors that of $\phi_{\Psi 500}$ but with weaker amplitude.

In general, the observational and model results in Figure 2 are qualitatively very similar, suggesting that the three metrics are appropriate not only for the observed climatology but also for the CMIP5 models'

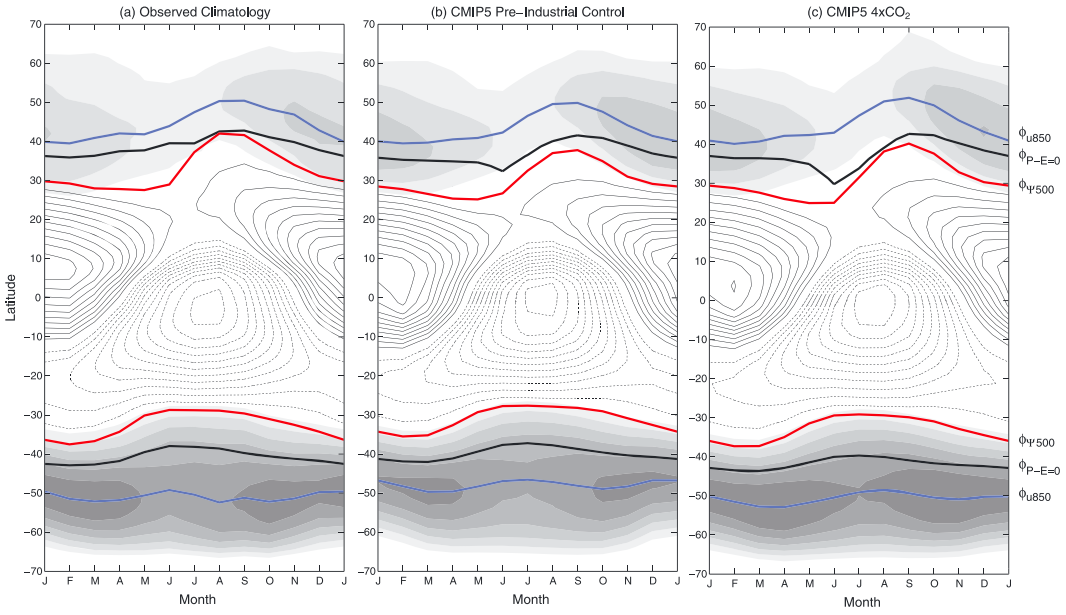

Figure 2. Monthly mean, zonal-mean values of (a) the 1979–2012 ERA-Interim reanalysis climatology, (b) the multimodel-mean CMIP5 preindustrial control climatology, and (c) the multimodel-mean CMIP5 4×CO_2 climatology. Gray shading denotes the 850 hPa zonal-mean zonal wind (contour interval: 2 m s^{-1}, for values ≥2 m s^{-1}), and thin black lines denote the 500 hPa mean meridional mass stream function (contour interval: 2.0×10^{10} kg s^{-1}; negative contours dashed and zero contour omitted). The locations of ϕ_{u850}, $\phi_{P-E=0}$, and $\phi_{\Psi 500}$ in each hemisphere are indicated by the thick blue, black, and red lines, respectively.

preindustrial control and 4×CO_2 climatologies examined in this study. One exception is NH $\phi_{P-E=0}$, which experiences a sharp equatorward shift in early summer in the models that is not present in observations. Because the NH branch of the Hadley circulation is very weak in summer, $\phi_{\Psi 500}$ and $\phi_{P-E=0}$ are less clearly defined during June–August, particularly in some CMIP5 models. As a result, readers should interpret the NH summer $\phi_{\Psi 500}$ and $\phi_{P-E=0}$ results with more caution.

3. Correlations Between Dynamical Sensitivity and Climate Sensitivity

In this section, we first introduce the magnitudes of our three metrics of dynamical sensitivity in CMIP5 models and then document their correlations with ECS. From Figures 2b and 2c, one might notice that ϕ_{u850}, $\phi_{P-E=0}$, and $\phi_{\Psi 500}$ are not the same in the preindustrial control and 4×CO_2 climates of CMIP5 models. As noted in section 1, with the addition of atmospheric CO_2, there appears to be a poleward shift in the multimodel-mean values of ϕ_{u850}, $\phi_{P-E=0}$, and $\phi_{\Psi 500}$ in both hemispheres during most seasons. This is shown more clearly in Figure 3.

Figure 3 shows the responses of ϕ_{u850}, $\phi_{P-E=0}$, and $\phi_{\Psi 500}$ to quadrupled atmospheric CO_2 concentrations in the 23 CMIP5 models listed in Table 1. For each metric, the results are shown for the annual mean as well as for the four seasonal means: December-January-February (DJF), March-April-May (MAM), June-July-August (JJA), and September-October-November (SON). In the SH, in nearly all models, ϕ_{u850}, $\phi_{P-E=0}$, and $\phi_{\Psi 500}$ shift poleward in all seasons in response to 4×CO_2 forcing (Figure 3, bottom row; see also Figure 2 of GP14). Most models cluster around a ~2° poleward shift in $\phi_{P-E=0}$ and $\phi_{\Psi 500}$ throughout the year, whereas the response of ϕ_{u850} has more intermodel spread. The most robust poleward SH jet shifts occur during the DJF and MAM seasons. The seasonality of these responses is consistent with previous studies [*Barnes and Polvani*, 2013; *Hu et al.*, 2013; GP14].

In the NH, in most models, ϕ_{u850} shifts poleward in all seasons, and $\phi_{P-E=0}$ and $\phi_{\Psi 500}$ shift poleward in all seasons but summer (Figure 3, top row). The most robust poleward shifts in the three metrics occur during the fall season (SON). In general, the NH responses are more widely scattered across models than in the SH, particularly for ϕ_{u850} in DJF and $\phi_{P-E=0}$ and $\phi_{\Psi 500}$ in JJA. The scatter in the NH ϕ_{u850} response reflects in part the competing responses from the jets in the Atlantic and Pacific basins [*Barnes and Polvani*, 2013; *Simpson et al.*, 2014; *Grise and Polvani*, 2014b], causing the NH zonal-mean jet to be broader and more difficult to define than its counterpart in the SH (see Figure 1); we address the contributions from the Atlantic and Pacific basins in further detail in section 4 (see Figures 8 and 9a). The scatter in the NH $\phi_{P-E=0}$ and $\phi_{\Psi 500}$ responses during JJA reflects the fact that these metrics are very poorly defined in NH summer due to the weak NH summer branch of the Hadley circulation (see section 2). Nonetheless, it is interesting that a large fraction of the models shift $\phi_{P-E=0}$ and $\phi_{\Psi 500}$ equatorward in JJA, as the weak NH summer branch of the Hadley circulation weakens even further in response to 4×CO_2 forcing (see also Figure 5c, top). As in the SH, the seasonality of the NH responses shown in Figure 3 is consistent with that shown in previous studies [*Barnes and Polvani*, 2013; *Hu et al.*, 2013].

We now ask what fraction of the intermodel spread in dynamical sensitivity (as shown in Figure 3) can be explained by the intermodel spread in ECS. To answer this question, Figure 4 presents correlations of 2×ECS with the responses of ϕ_{u850}, $\phi_{P-E=0}$, and $\phi_{\Psi 500}$ to 4×CO_2 forcing in each model, as shown by GP14 for the SH (see their Figure 3, reproduced here as Figure 4a). In the SH, the annual-mean poleward shifts in ϕ_{u850}, $\phi_{P-E=0}$, and $\phi_{\Psi 500}$ are significantly correlated with ECS. In the annual mean, the intermodel spread in ECS explains 59% (i.e., $r^2 = (-0.77)^2$) of the intermodel variance in the $\phi_{\Psi 500}$ response, 44% of the intermodel variance in the $\phi_{P-E=0}$ response, and 20% of the intermodel variance in the ϕ_{u850} response.

Furthermore, we find that the shift in $\phi_{\Psi 500}$ is significantly correlated with ECS during all seasons, whereas the shifts in ϕ_{u850} and $\phi_{P-E=0}$ are only significantly correlated with ECS during DJF and MAM. For example, the intermodel spread in ECS explains 25% of the intermodel variance in the austral summer ϕ_{u850} response (consistent with the findings of *Gerber and Son* [2014]) but only 6% of the intermodel variance in the austral winter ϕ_{u850} response. During DJF and MAM, the interannual variability and global warming responses of ϕ_{u850} and $\phi_{P-E=0}$ have been shown to be tightly coupled to those of $\phi_{\Psi 500}$ [*Lu et al.*, 2008; *Kang and Polvani*, 2011], and GP14 suggested that this might be the reason why all three metrics are significantly correlated with ECS during

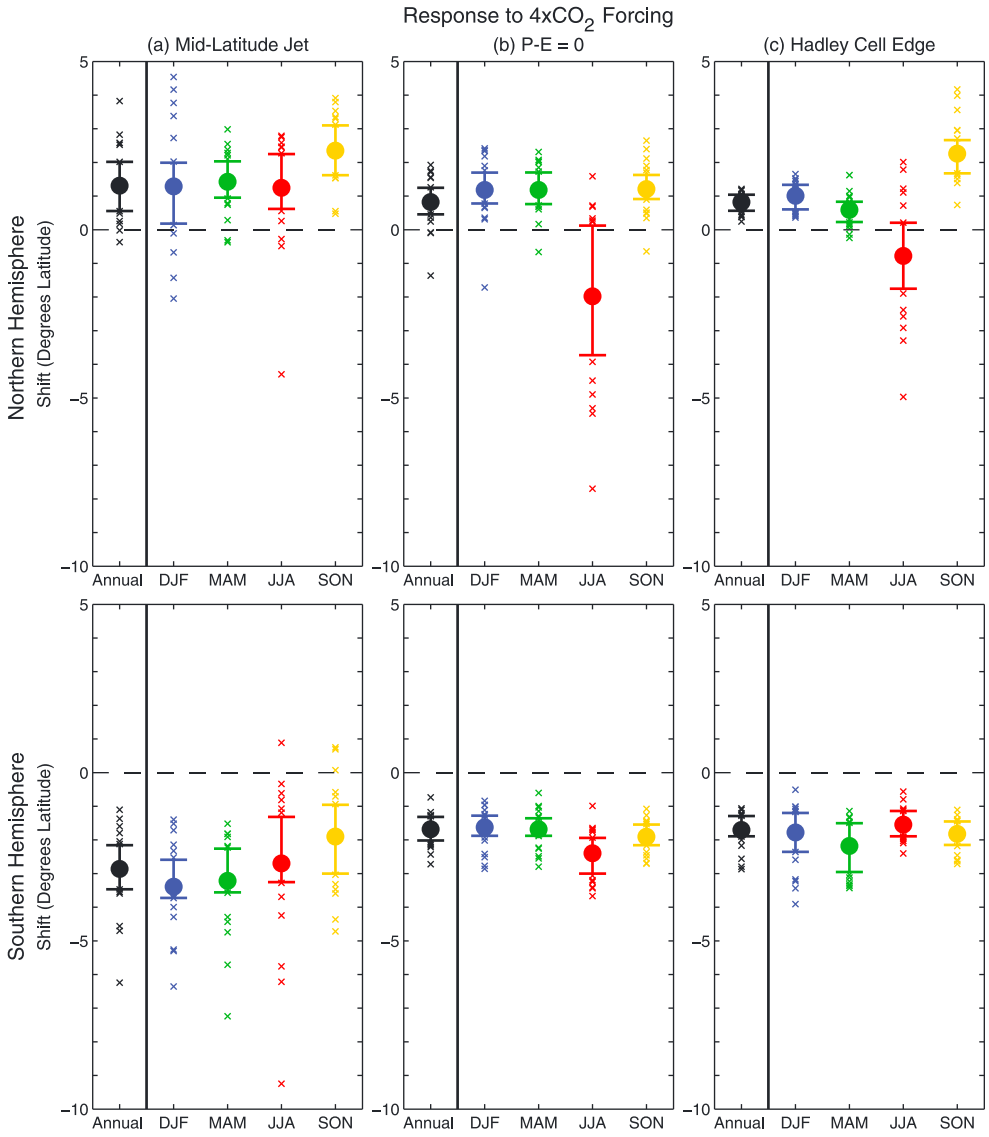

Figure 3. Magnitude of the shift in the (a) midlatitude jet (ϕ_{u850}), (b) subtropical dry zone ($\phi_{P-E=0}$), and (c) Hadley cell edge ($\phi_{\Psi 500}$) in response to 4×CO_2 forcing in the 23 CMIP5 models listed in Table 1, for the (top row) Northern Hemisphere and (bottom row) Southern Hemisphere. For each season, the multimodel mean is denoted by large dots, the range of the 25th–75th percentiles are denoted by thick horizontal bars, and the outliers about the 25th–75th percentiles are denoted by crosses.

these seasons. In contrast, during JJA and SON, GP14 found that the shifts in ϕ_{u850} and $\phi_{P-E=0}$ are instead more strongly linked to biases in the preindustrial control climatology (see their Figure 4).

In the NH, the responses of ϕ_{u850} and $\phi_{P-E=0}$ are not significantly correlated with ECS during any season (Figure 4b, top and middle plots). In the annual mean, the intermodel spread in ECS explains less than 3% of the intermodel variance in the ϕ_{u850} and $\phi_{P-E=0}$ responses. However, as noted above, the response of ϕ_{u850} reflects competing behavior from the Atlantic and Pacific basins. For example, models with higher ECS tend to shift the North Pacific jet further equatorward during JJA and the North Atlantic jet further poleward during SON (see Figure 9b). We discuss this behavior further in the next section.

The annual-mean poleward shift of NH $\phi_{\Psi 500}$ is also not significantly correlated with ECS (Figure 4b, bottom), and the intermodel spread in ECS only explains 7% of the intermodel variance in the annual-mean NH $\phi_{\Psi 500}$ response. This is particularly surprising, given the significant relationship between $\phi_{\Psi 500}$ and ECS in all seasons in the SH. In fact, one would anticipate a strong relationship between $\phi_{\Psi 500}$ and ECS, given that (1)

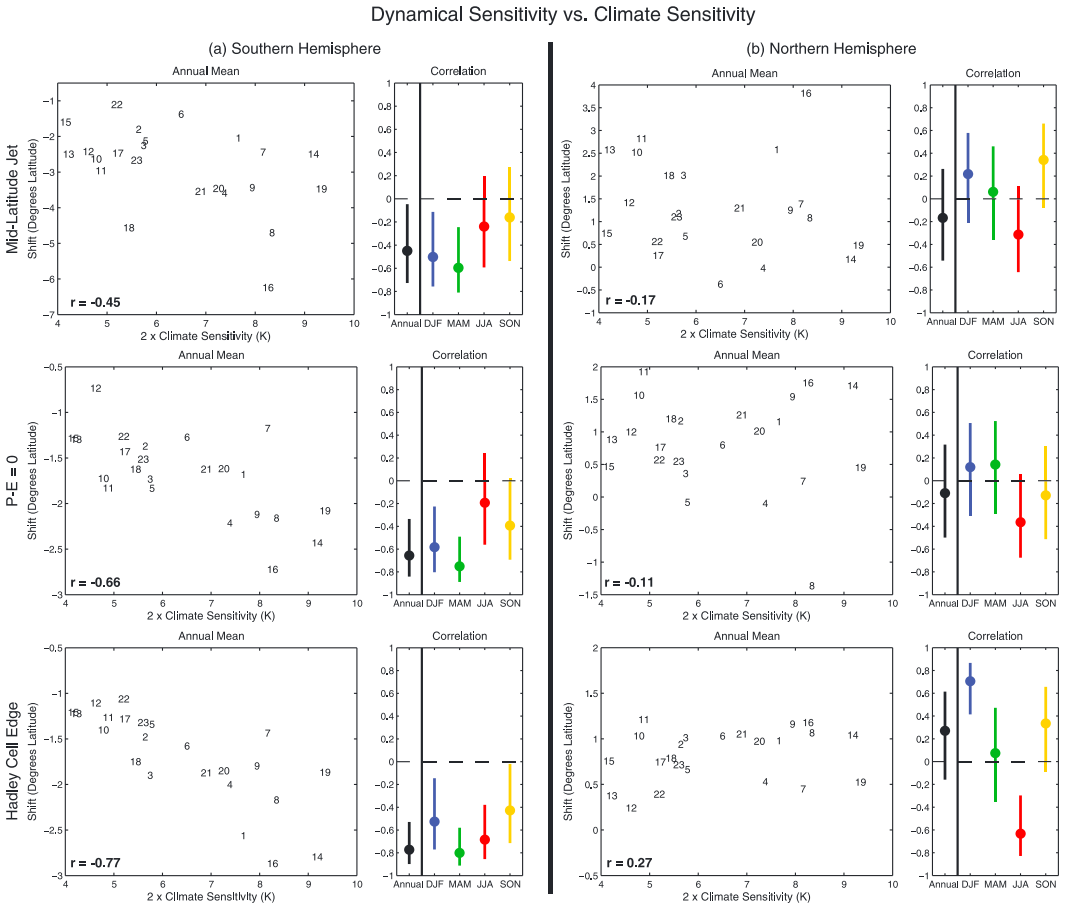

Figure 4. Scatterplots of three annual-mean metrics of dynamical sensitivity ((top row) ϕ_{u850}, (middle row) $\phi_{P-E=0}$, and (bottom row) $\phi_{\Psi 500}$) with twice the equilibrium climate sensitivity of each model for (a) the Southern Hemisphere and (b) the Northern Hemisphere. The numbers in each scatterplot corresponded to the numbered CMIP5 models in Table 1. Next to each scatterplot, correlations between the metrics of dynamical sensitivity and climate sensitivity are plotted for the annual mean and the four seasonal means. Error bars denote the 95% confidence bounds on the correlation coefficients.

variability in $\phi_{\Psi 500}$ is closely tied to tropical-mean surface temperatures (e.g., in the case of the El Niño–Southern Oscillation [*Seager et al.*, 2003; *Lu et al.*, 2008]) and that (2) the tropical-mean surface temperature response to CO_2 forcing is highly correlated with ECS ($r \approx 0.90$, as found in GP14). On closer inspection, the shift in NH $\phi_{\Psi 500}$ does indeed have a robust relationship with ECS: a significant positive correlation in DJF and a significant negative correlation in JJA that largely cancel in the annual mean. Although NH $\phi_{\Psi 500}$ is poorly defined during JJA, it seems highly unlikely that such a strong negative correlation with ECS would arise by chance, suggesting that models with larger ECS do indeed have a larger equatorward shift in NH $\phi_{\Psi 500}$ during JJA.

In summary, Figure 4 illustrates that models with higher values of ECS tend to shift SH $\phi_{\Psi 500}$ further poleward during all seasons, SH ϕ_{u850} and $\phi_{P-E=0}$ further poleward during DJF and MAM, and NH $\phi_{\Psi 500}$ further poleward in DJF and further equatorward in JJA. We note that these results are in some contrast to those reported by *Vallis et al.* [2015], who found little relationship between climate sensitivity and the annual-mean response to CO_2 forcing for both the Hadley cell edge and midlatitude jet latitude in both hemispheres. However, *Vallis et al.* [2015] use a different metric for climate sensitivity (TCR instead of ECS), different metrics for the Hadley cell edge and midlatitude jet latitude (based on the surface wind field), and a different subset of CMIP5 models. In the subset of models used here, the correlations in the SH are in fact somewhat smaller when TCR and the surface wind metrics are used (not shown).

Overall, the fact that some metrics of dynamical sensitivity correlate strongly with ECS is not necessarily surprising, given that many of the physical mechanisms proposed to explain dynamical sensitivity are closely

related to the global-mean surface temperature response (as described in section 1). More interesting is that a large fraction of the intermodel spread in dynamical sensitivity appears unrelated to the intermodel spread in ECS. In the next section, we seek further insight into these results by examining the role of ECS in the entire zonal-mean global circulation response to 4×CO_2 forcing.

4. Decomposition of the Zonal-Mean Global Circulation Response

To better understand the correlations between our three metrics of dynamical sensitivity and ECS (as documented in the previous section), we now extend our analysis to the entire zonal-mean global circulation response. To do this, for each model, we partition the response of a field X to 4×CO_2 forcing using the following equation:

$$X_{4\times CO2} = X_{\text{control}} + a(\text{ECS}) + b \tag{1}$$

where a is the linear regression coefficient between ECS and the response of X to 4×CO_2 forcing (i.e., $X_{4\times CO2} - X_{\text{control}}$) calculated using all models. Thus, for each model, the component of the response of X to 4×CO_2 forcing that is linearly congruent with the intermodel spread in ECS is given by the product of a and that model's ECS, and the component of the response of X that is linearly independent of the intermodel spread in ECS is given by the residual b. Results of this decomposition for the mean meridional stream function, precipitation minus evaporation, and zonal wind fields are shown in Figures 5–7.

The top row of Figure 5 shows the CMIP5 multimodel mean response of the mean meridional stream function to 4×CO_2 forcing (i.e., $X_{4\times CO2} - X_{\text{control}}$ from equation (1), averaged over all models), the middle row of Figure 5 shows the component of this response that is linearly congruent with the intermodel spread in ECS (i.e., the product of a and ECS from equation (1), averaged over all models), and the bottom row of Figure 5 shows the residual (i.e., b from equation (1), averaged over all models). In the SH, consistent with the correlations in Figure 4, most components of the mean meridional circulation response to CO_2 forcing are linearly congruent with ECS, including (1) the poleward shift of the Ferrel cell (near 60°S), (2) the upward and poleward expansion of the Hadley circulation (between the equator and 30°S), and (3) the weakening of the cross-equatorial branch of the Hadley circulation during JJA. As discussed in section 1, the poleward expansion of the circulation is plausibly linked to global-mean surface temperature warming via the moist adiabatic adjustment of tropospheric lapse rates to surface warming [*Frierson et al.*, 2007; *Butler et al.*, 2010; *Gerber and Son*, 2014], and the weakening of the Hadley circulation is plausibly linked to global-mean surface temperature warming through increasing water vapor via the Clausius-Clapeyron relationship [*Held and Soden*, 2006]. The upward expansion of the circulation is consistent with the rising of the tropopause height in a warming climate [*Santer et al.*, 2003; *Lorenz and DeWeaver*, 2007; *Vallis et al.*, 2015].

In the NH, likewise, the upward and poleward expansion of the Hadley circulation (between the equator and 30°N) is linearly congruent with ECS during DJF. However, in the NH, there are larger differences between the total mean meridional stream function response to CO_2 forcing (Figure 5, top row) and the component that is linearly congruent with ECS (Figure 5, middle row). Of particular interest is that the total response of the NH summer Hadley circulation (~20°N–30°N) to 4×CO_2 forcing is characterized by weakening (Figure 5c, top) but that models with larger values of ECS instead contract the Hadley circulation equatorward during summer months (Figure 3c, top; Figure 4b, bottom; and Figure 5c, middle). Consistent with these results, *Shaw and Voigt* [2015] recently showed that, in CMIP5 experiments forced with sea surface temperature (SST) warming alone (i.e., with no change in atmospheric composition), the tropical circulation contracts equatorward in the Asian-Pacific sector during NH summer. Given that most global-mean surface temperature warming (and hence ECS) consists of SST changes, it is not surprising that the SST-mediated response isolated by *Shaw and Voigt* [2015] is similar to the ECS-congruent response shown here in Figure 5 (middle row). The spatial pattern of SST warming may be particularly important in determining whether the Hadley cell edge expands poleward or contracts equatorward, as a tropical warming of narrow meridional extent has been shown to produce an equatorward contraction of the Hadley cell edge in model experiments [*Chen et al.*, 2010; *Tandon et al.*, 2013; *He and Soden*, 2015].

The nonnegligible component of the mean meridional circulation response to CO_2 forcing that is not congruent with ECS (Figure 5, bottom row) suggests that additional mechanisms (independent of ECS) must exist to explain the intermodel spread in (1) the response of the strength of the Hadley circulation to CO_2 forcing and (2) the behavior of the NH summer Hadley cell edge (Figure 5c, bottom). Consistent with these results, *He and Soden* [2015] and *Shaw and Voigt* [2015] recently showed that, in CMIP5 experiments forced with quadrupled

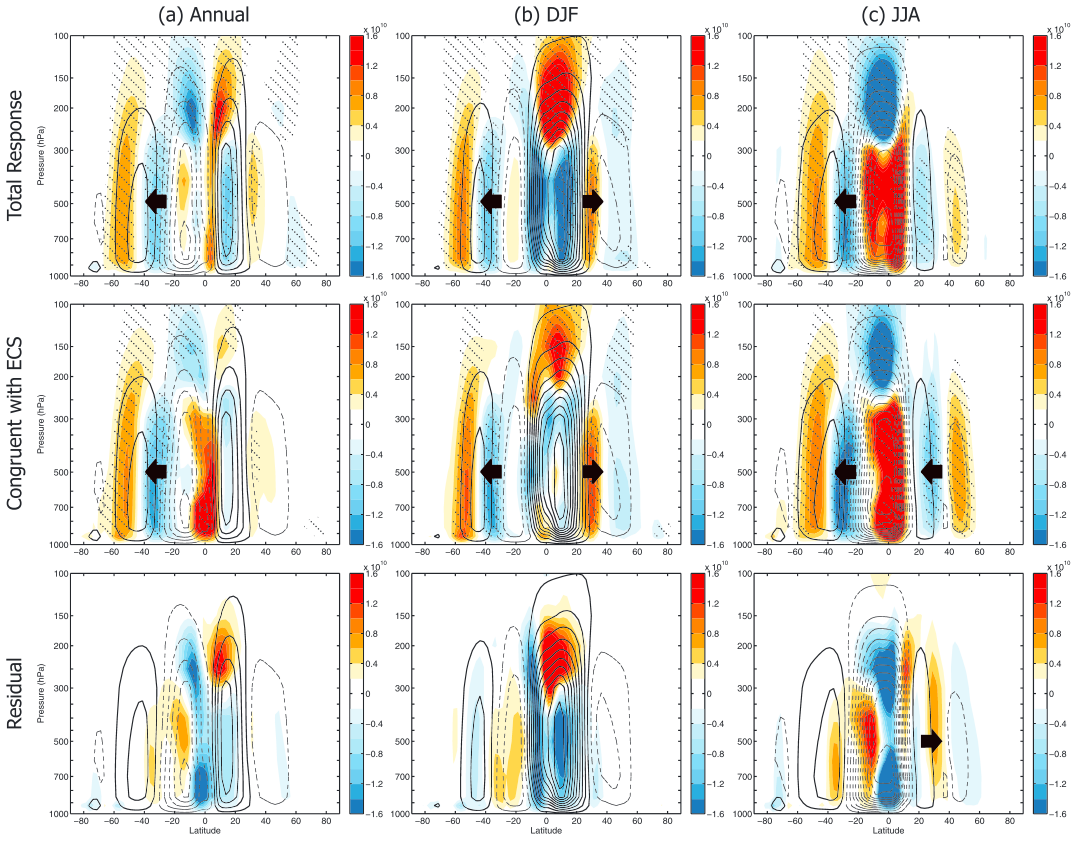

Figure 5. CMIP5 multimodel-mean response of the mean meridional mass stream function to 4×CO_2 forcing (shading interval: 2.0×10^9 kg s^{-1}) for the (a) annual mean, (b) December-January-February (DJF) mean, and (c) June-July-August (JJA) mean. (top row) The total response, (middle row) the component of the total response that is linearly congruent with equilibrium climate sensitivity (ECS), and (bottom row) the residual are shown. For reference, the line contours in each plot show the preindustrial control climatology (contour interval: 2.0×10^{10} kg s^{-1}; solid: positive and dashed: negative). Stippling in the first and second rows indicates where the response is 95% statistically significant via Student's *t* test. Bold arrows illustrate the movement of the poleward edges of the Hadley circulation.

CO_2 concentrations (but with no change in SSTs and thus little change in global-mean surface temperature), modest weakening of the NH Hadley circulation occurs (see Figure 10c of *He and Soden* [2015]), and the tropical circulation expands poleward in the Asian-Pacific sector during NH summer [*Shaw and Voigt*, 2015]. By fixing SSTs and changing atmospheric CO_2, these experiments isolate the direct radiative effects of CO_2 on

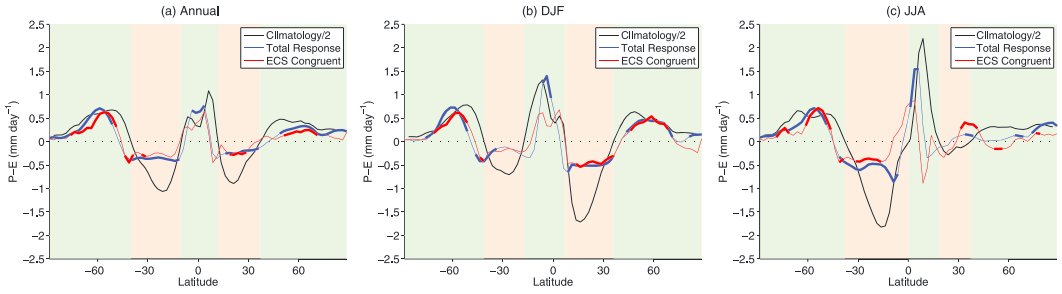

Figure 6. CMIP5 multimodel-mean response of zonal-mean precipitation minus evaporation ($P - E$) to 4×CO_2 forcing for (a) annual mean, (b) DJF mean, and (c) JJA mean. The total response is plotted in blue, and its component that is linearly congruent with equilibrium climate sensitivity is plotted in red. The blue and red lines are thicker where the response is 95% statistically significant via Student's *t* test. For reference, the black line in each plot shows the multimodel-mean climatology for the CMIP5 preindustrial control climate (divided by a factor of 2 for plotting purposes). Regions where climatological $P - E > 0$ are shaded in green, and regions where climatological $P - E < 0$ are shaded in brown.

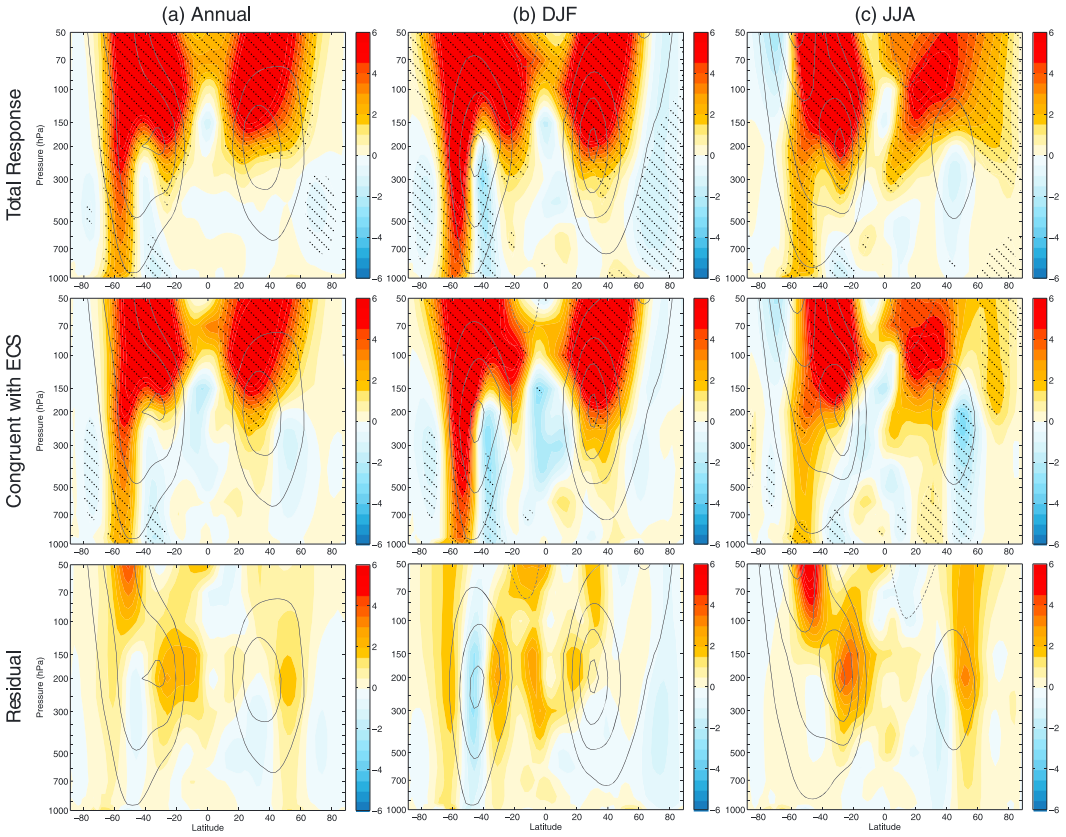

Figure 7. (a–c) Same as in Figure 5 but for the multimodel-mean response of the zonal-mean zonal wind to 4×CO_2 forcing (shading interval: 0.5 m s^{-1}). The line contours in each plot show the preindustrial control climatology (contour interval: 10 m s^{-1}; solid: positive and dashed: negative).

the atmospheric circulation but also include changes in atmospheric circulation patterns (e.g., stationary waves) due to a modest warming of the land surface. It seems plausible that these effects could contribute to the residual circulation responses documented here (Figure 5c, bottom), as they are largely independent of global-mean surface temperature warming. Further discussion of the mechanisms responsible for the residual circulation response is provided in section 5.

In Figure 6, we plot the multimodel mean response of zonal-mean precipitation minus evaporation to 4×CO_2 forcing (in blue), along with the component of the response that is linearly congruent with ECS (in red). For reference, we also plot the multimodel-mean climatology from the preindustrial control climate of the models (in black, scaled by a factor of 2). Consistent with the results discussed above, many components of the SH precipitation minus evaporation response to CO_2 forcing are linearly congruent with ECS, including (1) the strengthening of the midlatitude storm track precipitation (poleward of ~40°S), (2) the poleward shift of the maximum midlatitude storm track precipitation (near ~50°S) in the annual mean and DJF (see also Figure 3a, bottom and Figure 4a, top), (3) the poleward expansion of the subtropical dry zone (near ~40°S) in the annual mean and DJF (see also Figure 3b, bottom and Figure 4a, middle), and (4) the strengthening of the subtropical dry zone (equatorward of ~40°S) in JJA (Figure 6c). As discussed above, the poleward shift of the midlatitude storm track precipitation and subtropical dry zone is plausibly linked to the global-mean surface temperature warming via the moist adiabatic adjustment of tropospheric lapse rates to surface warming [e.g., *Frierson et al.*, 2007], and the intensification of the midlatitude storm track precipitation and subtropical dry zone (the so-called "wet get wetter, dry get drier" response) follows directly from increased water vapor transport in a warmer world via the Clausius-Clapeyron relationship [*Held and Soden*, 2006; *Seager et al.*, 2010]. In the NH, likewise, the strengthening of the midlatitude storm track precipitation and subtropical dry zone are linearly congruent with ECS in DJF (Figure 6b). However, the total NH precipitation minus evaporation response in JJA bears little resemblance to its ECS-congruent component (Figure 6c, compare red and blue lines).

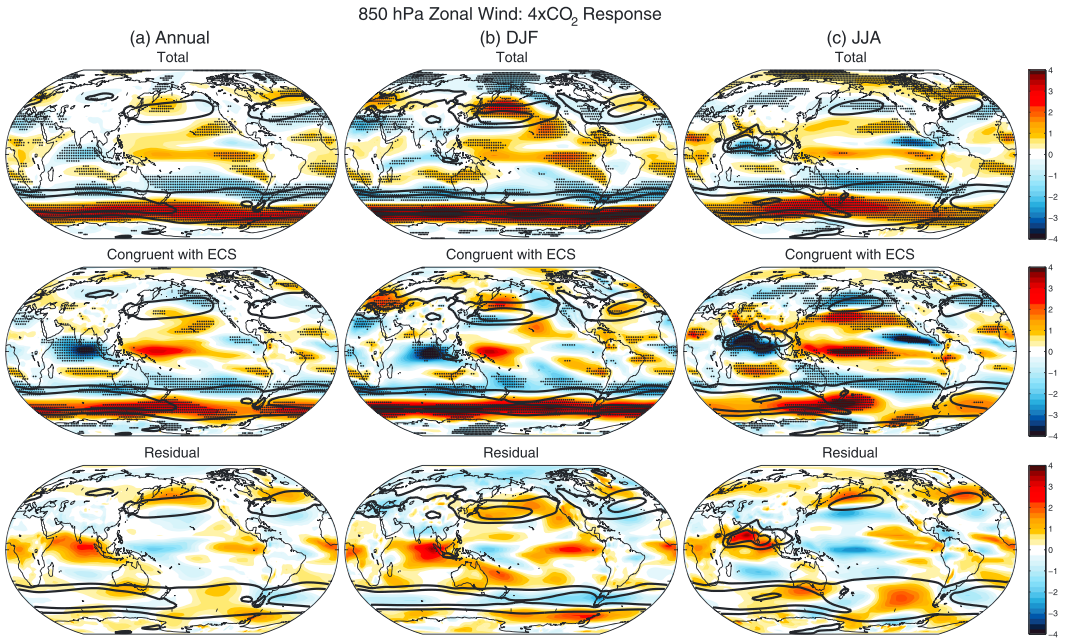

Figure 8. (a–c) Same as in Figure 5 but for the multimodel-mean response of the 850 hPa zonal wind to 4×CO_2 forcing (contour interval: 0.25 m s^{-1}). The thick contours outline the preindustrial control climatology (contour interval: 5 m s^{-1}).

In Figure 7, we plot the multimodel mean response of the zonal-mean zonal wind to 4×CO_2 forcing, as well as the components of the response that are linearly congruent with and independent of the intermodel spread in ECS. In response to 4×CO_2 forcing, zonal winds in the subtropical and midlatitude upper troposphere and lower stratosphere significantly strengthen during all seasons. This feature is highly congruent with ECS, as global-mean surface temperature rise is strongly tied to tropical upper tropospheric warming (via the moist adiabatic adjustment of tropical tropospheric lapse rates) and thus to the strength of the equator-to-pole temperature gradient in the upper troposphere-lower stratosphere.

In the lower troposphere, the zonal-mean zonal wind response to 4×CO_2 forcing is dominated by a poleward shift and strengthening of the SH midlatitude jet [e.g., *Barnes and Polvani*, 2013], which is largely congruent with ECS (most significantly in the annual mean and DJF; Figure 3a, bottom and Figure 4a, top). The poleward shift of the tropospheric jet has also been linked to global-mean surface temperature warming via the moist adiabatic adjustment of tropospheric lapse rates to surface warming [*Butler et al.*, 2010; *Arblaster et al.*, 2011; *Gerber and Son*, 2014]. As noted by *Grise and Polvani* [2014b], the multimodel-mean, zonal-mean zonal wind response in the NH midlatitude lower troposphere is much weaker and not statistically significant, reflecting the larger uncertainty in the NH jet response across models (Figure 3a, top). Interestingly, models with larger values of ECS tend to contract the NH midlatitude jet equatorward during JJA (Figure 7c, middle). This result might seem counterintuitive, given that in nearly all models the NH midlatitude jet shifts poleward during JJA (Figure 3a, top). However, the pattern in Figure 7c is consistent with the small negative correlation in Figure 4 b (top), as models that shift the NH summertime jet the most poleward tend to be the ones with the smallest values of ECS. Hence, the sign of the relationship between ECS and dynamical sensitivity need not be the same as the sign of the multimodel-mean circulation response.

To better understand the lower tropospheric zonal-mean zonal wind response to 4×CO_2 forcing in Figure 7, we now examine the longitudinal structure of the zonal wind response. In Figure 8, we plot the response of the 850 hPa zonal wind to 4×CO_2 forcing, as well as its components that are linearly congruent with and independent of ECS. In response to 4×CO_2 forcing, the SH jet shifts poleward during all seasons at nearly all longitudes [*Simpson et al.*, 2014; *Grise and Polvani*, 2014b]. The SH jet shift is largely congruent with ECS (consistent with Figures 3, 4, and 7 above), particularly during DJF when the jet is very zonally symmetric. In the NH, the zonal-mean jet response (as shown in Figures 3, 4, and 7) masks complex and competing effects arising from the North Atlantic and North Pacific basins.

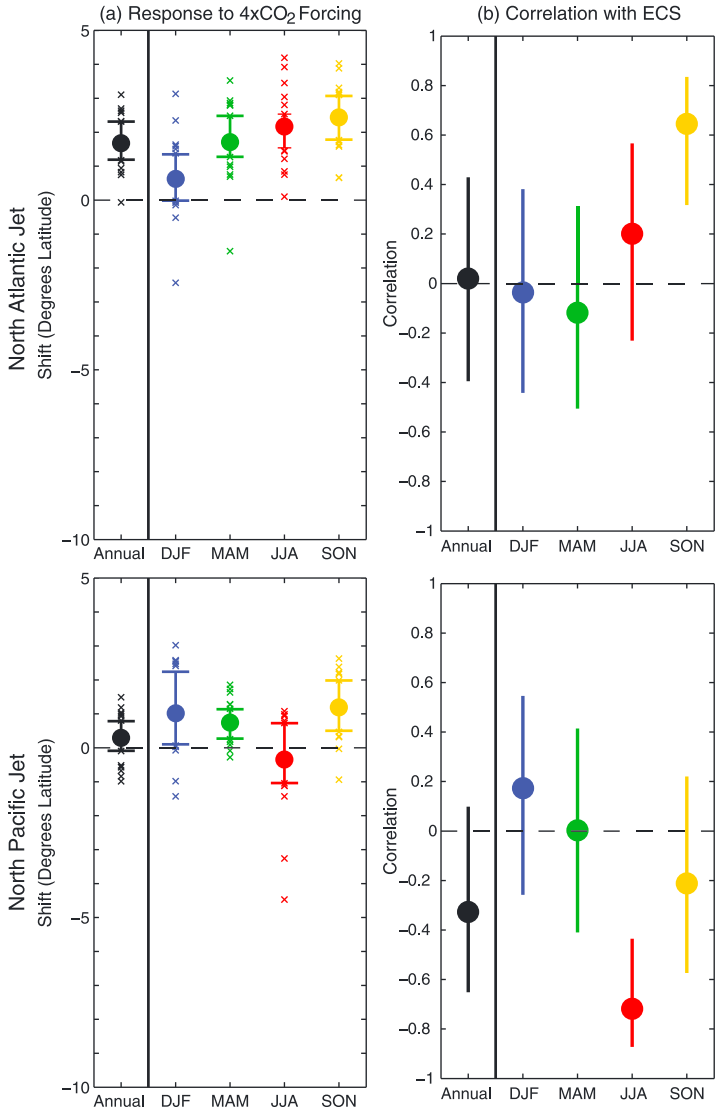

Figure 9. (a) Same as in Figure 3 but for the (top) North Atlantic (300°E–0°E) and (bottom) North Pacific (135°E–235°E) midlatitude jets. The latitudes of the North Atlantic and North Pacific midlatitude jets are found using the same method as ϕ_{u850}, except that the zonal wind is averaged over the designated longitude range (instead of all longitudes). (b) Same as in Figure 4 but for the (top) North Atlantic jet and (bottom) the North Pacific jet.

The North Atlantic jet shifts robustly poleward in all seasons but DJF (Figure 9a, top), when the zonal wind response is limited to the climatological jet exit region [*Harvey et al.*, 2012; *Simpson et al.*, 2014; *Grise and Polvani*, 2014b]. Moreover, the poleward shift of the North Atlantic jet is only significantly correlated with ECS during SON (Figure 9b, top); instead, the residual component largely explains the poleward shift of the North Atlantic jet during other seasons (Figure 8, bottom). In contrast, the North Pacific jet only shifts robustly poleward during SON (Figure 9a, bottom; see also Figure 2 of *Grise and Polvani* [2014b]). During other seasons, the 850 hPa zonal wind response over the North Pacific is characterized by a quadrapole pattern (DJF) and an equatorward shift (JJA) (Figure 8, top) [*Simpson et al.*, 2014; *Grise and Polvani*, 2014b]. These complicated responses are congruent with ECS (Figure 8, middle); the residual component contributes to a poleward shift of the Pacific jet in the annual mean and JJA and a strengthening of the Pacific jet in DJF (Figure 8, bottom). The complicated nature of the ECS-congruent component of the 850 hPa zonal wind response in the NH likely reflects systematic changes in NH stationary wave patterns in a warming climate across CMIP5 models (see *Simpson et al.* [2014] for a detailed discussion).

The decomposition of the 850 hPa zonal wind response to 4×CO_2 forcing shown in Figure 8 is reminiscent of that made by *Grise and Polvani* [2014b] (see their Figure 3). Using similar methodology to the *He and Soden* [2015] and *Shaw and Voigt* [2015] studies discussed above, *Grise and Polvani* [2014b] decomposed the 850 hPa zonal wind response using CMIP5 experiments forced by SST increases only (i.e., with fixed atmospheric composition) and CO_2 increases only (i.e., with fixed SSTs). The ECS-congruent response shown here in Figure 8 (middle row) bears some resemblance to the SST-mediated response of *Grise and Polvani* [2014b], again suggesting that warming SSTs are linked to the mechanisms responsible for the ECS-congruent response. The residual response shown here in Figure 8 (bottom row) is instead more similar to the circulation response to CO_2 increases with fixed SSTs (cf. Figures 3 and 4 of *Grise and Polvani* [2014b]).

To summarize, in this section, we have decomposed the zonal-mean global circulation response of CMIP5 models to 4×CO_2 forcing into two components, one linearly congruent with the intermodel spread in ECS and one linearly independent of the intermodel spread in ECS. Corroborating the results from section 3, we found that many aspects of the atmospheric circulation response to CO_2 forcing in the SH are linearly congruent with ECS, whereas the majority of the NH circulation response is linearly independent of ECS. As discussed above, many mechanisms proposed to explain the atmospheric circulation response to increased CO_2 concentrations have a direct link to global-mean surface temperature rise, which arises in large part from SST increases. If such mechanisms are shared collectively across CMIP5 models, then they would be reflected in the ECS-congruent responses shown in this section. The remaining residual component of the circulation response must therefore be driven by mechanisms unrelated to the intermodel spread in ECS. In the next section, we provide further discussion of potential physical mechanisms responsible for the ECS-congruent and residual components of dynamical sensitivity.

5. Discussion

In this section, we investigate four potential physical mechanisms—already mentioned in the Introduction—that could be responsible for the intermodel spread in dynamical sensitivity: (1) increased subtropical static stability ($\theta_{400\ \mathrm{hPa}}$–$\theta_{850\ \mathrm{hPa}}$, averaged over 20°–40° latitude), (2) increased midlatitude static stability ($\theta_{400\ \mathrm{hPa}}$–$\theta_{850\ \mathrm{hPa}}$, averaged over 40°–60° latitude), (3) increased upper tropospheric-lower stratospheric equator-to-pole temperature gradient ($T_{0°–30°\ \mathrm{latitude}}$–$T_{60°–90°\ \mathrm{latitude}}$ at 200 hPa), and (4) decreased surface equator-to-pole temperature gradient ($T_{0°–30°\ \mathrm{latitude}}$–$T_{60°–90°\ \mathrm{latitude}}$ at surface). As described in section 1, the first three mechanisms are physically linked to the global-mean surface temperature. Hence, not surprisingly, the intermodel spread in the magnitude of the response of these three mechanisms to 4×CO_2 forcing is significantly correlated with the intermodel spread in ECS (Table 2, top three rows), and it is likely that these mechanisms play an integral role in driving the ECS-congruent component of dynamical sensitivity highlighted in sections 3 and 4. Consistent with these findings, we find few significant correlations between these three mechanisms and the residual (ECS-independent) component of our three metrics of dynamical sensitivity (ϕ_{u850}, $\phi_{P-E=0}$, and $\phi_{\Psi 500}$; not shown).

In contrast, the intermodel spread in the magnitude of the surface equator-to-pole temperature gradient response to 4×CO_2 forcing is more weakly correlated with the intermodel spread in ECS, particularly in the SH (Table 2, bottom row). However, we find stronger evidence that the surface meridional temperature gradient response is linked to the residual component of dynamical sensitivity, again particularly in the SH. Figure 10 plots the correlations of the residual responses of ϕ_{u850}, $\phi_{P-E=0}$, and $\phi_{\Psi 500}$ to 4×CO_2 forcing (i.e., b in equation (1)) with the response of the equator-to-pole surface temperature gradient to 4×CO_2 forcing for all models. In these plots, a positive (negative) correlation implies that a strengthening equator-to-pole surface temperature gradient is linked to a greater poleward shift in ϕ_{u850}, $\phi_{P-E=0}$, or $\phi_{\Psi 500}$ in the NH (SH).

In the NH, almost all the correlations between the residual component of dynamical sensitivity and the equator-to-pole surface temperature gradient response are not statistically significant (Figure 10, top row); only the residual ϕ_{u850} response in JJA is significantly correlated with the meridional surface temperature gradient response. In contrast, in the SH, a number of correlations between the residual component of dynamical sensitivity and the equator-to-pole surface temperature gradient response are statistically significant (Figure 10, bottom row). For example, a greater poleward shift in SH ϕ_{u850} is significantly correlated with a strengthening meridional surface temperature gradient during all seasons but MAM (Figure 10d), and a greater poleward shift in SH $\phi_{P-E=0}$ is significantly correlated with a strengthening meridional surface

Table 2. Correlations Between ECS and the Magnitude of the Responses of the Listed Mechanisms to 4×CO_2 Forcing[a]

Mechanism	Definition	Southern Hemisphere	Northern Hemisphere
Subtropical static stability	$\theta_{400\ hPa}-\theta_{850\ hPa}$ (averaged over 20°–40° latitude)	0.81	0.81
Midlatitude static stability	$\theta_{400\ hPa}-\theta_{850\ hPa}$ (averaged over 40°–60° latitude)	0.77	0.71
Upper tropospheric-lower stratospheric equator-to-pole temperature gradient	$T_{0°–30°\ latitude}-T_{60°–90°\ latitude}$ (200 hPa)	0.84	0.82
Surface equator-to-pole temperature gradient	$T_{0°–30°\ latitude}-T_{60°–90°\ latitude}$ (surface)	−0.18	−0.53

[a]All values are for the annual mean and derived from the CMIP5 models listed in Table 1.

temperature gradient during JJA and SON (Figure 10e). Note that, with the exception of SH ϕ_{u850} in DJF, these seasons are when the responses of SH ϕ_{u850} and SH $\phi_{P-E=0}$ are not significantly correlated with ECS (Figure 4a), indicating that the surface temperature gradient response might be more important in governing dynamical sensitivity during these seasons.

In a related study, *Ceppi et al.* [2014] recently found a strong linkage in CMIP5 models among the 21st century projected changes in SH ϕ_{u850}, the meridional gradient of SH midlatitude surface temperatures, and the meridional gradient of SH midlatitude absorbed solar radiation, which they attributed to uncertainties in future cloud and sea ice changes at these latitudes. The results in Figure 10 support a linkage between the SH ϕ_{u850} and meridional surface temperature gradient responses. However, the correlations in Figure 10 are not strongest during the season with the largest incoming solar radiation (DJF) but rather during seasons with the maximum sea ice extent along the Antarctic coastline in the preindustrial control climatology (JJA and SON; see Figure 1b of *Polvani and Smith* [2013]). Furthermore, we find a significant correlation ($r \approx 0.60$) between the magnitudes of the SH meridional surface temperature gradient response to 4×CO_2 forcing and the *clear-sky* shortwave feedback parameter (as listed in Table 1 of *Forster et al.* [2013]) for the 23 CMIP5 models examined here. *Deser et al.* [2015] and *Harvey et al.* [2015] have recently pointed to the importance of Arctic sea ice loss in understanding the NH wintertime circulation response in models, and it seems plausible that changes in Antarctic sea ice might also impact the SH wintertime circulation response. Future work will need to explore this issue in further detail.

Finally, in section 4, we noted that there was some resemblance between the residual (ECS-independent) component of the atmospheric circulation response to CO_2 forcing (Figures 5–8) and the atmospheric circulation response to CO_2 forcing with fixed SSTs (as documented by *Grise and Polvani* [2014b], *He and Soden* [2015], and *Shaw and Voigt* [2015]). From this comparison, one might expect that the intermodel spread in the direct radiative effects of CO_2 would be an important factor in explaining the residual component of dynamical sensitivity. Unfortunately, we find few significant correlations between the residual components of dynamical sensitivity and the adjusted radiative forcings of the models (as listed in Table 1 of *Forster et al.* [2013]), highlighting the complexity of the problem.

Overall, our results suggest that the intermodel spread in the global-mean surface temperature response to CO_2 forcing is strongly linked to the intermodel variability in the atmospheric circulation response, particularly in the SH. This is consistent with many of the mechanisms proposed by previous studies, including—but not limited to—increases in static stability and the upper tropospheric-lower stratospheric meridional temperature gradient, which are directly related to global-mean surface temperature increases (Table 2). Nonetheless, the residual component of dynamical sensitivity (i.e., the component of the circulation response that is independent of the intermodel spread in ECS) is nonnegligible, particularly in the NH. In this section, we have shown that changes to the meridional surface temperature gradient (such as via the sea ice response) might be important in explaining some fraction of the residual intermodel spread in the atmospheric circulation response in the SH. However, there are likely many additional mechanisms that contribute to the intermodel spread in the residual component of dynamical sensitivity, which we have not considered here. Furthermore, it is important to note that mechanisms unique to individual models (which could be proportional to global-mean temperature rise within those models) would be included in the residual component of dynamical

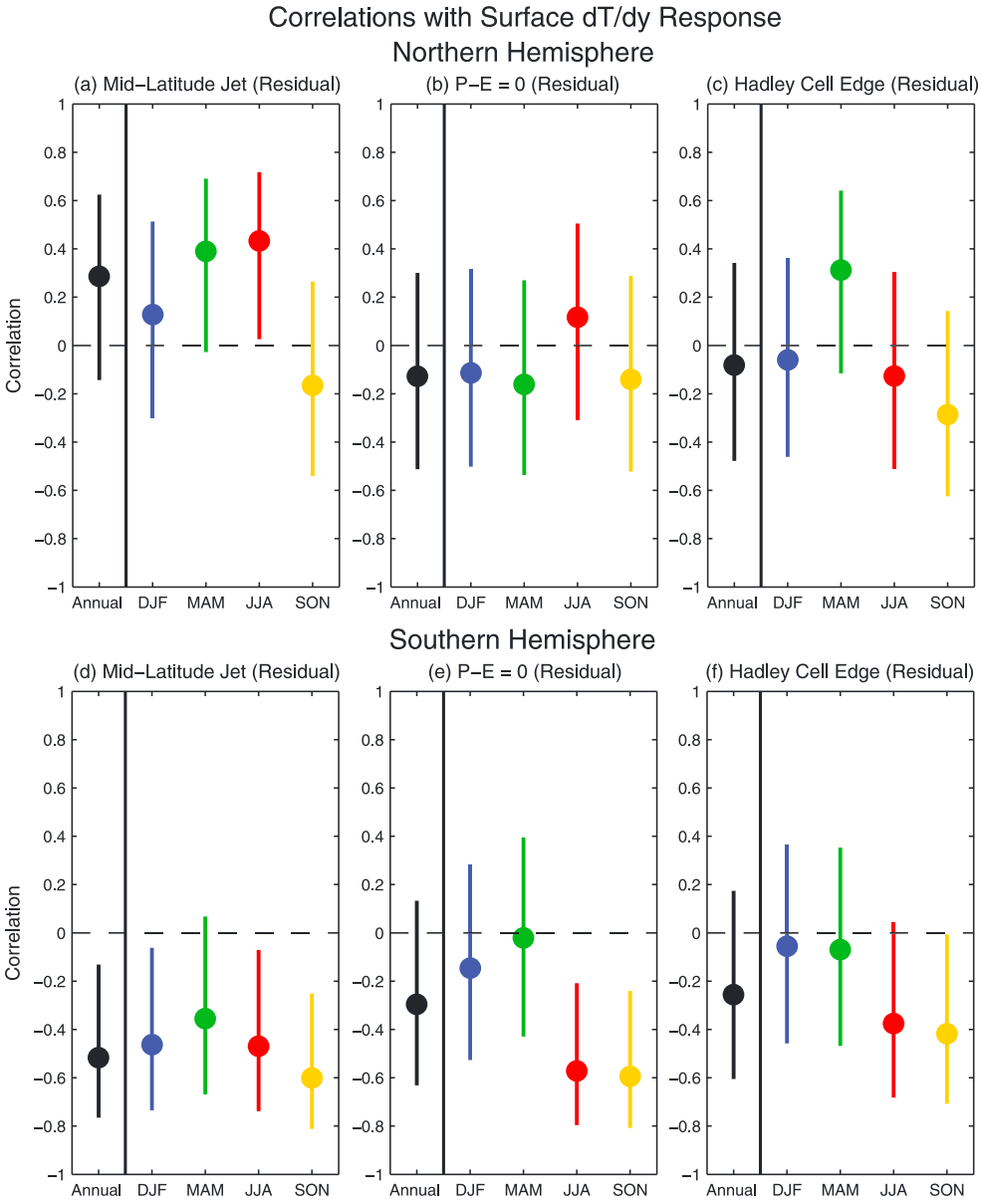

Figure 10. Correlations of the residual components of dynamical sensitivity ((a and d) ϕ_{u850}, (b and e) $\phi_{P-E=0}$, and (c and f) $\phi_{\Psi 500}$) with the response of the equator-to-pole surface temperature gradient (i.e., the 0°–30° latitude averaged temperature minus the 60°–90° latitude averaged temperature) to 4×CO_2 forcing for (top row) NH and (bottom row) SH. In the top (bottom) row, positive (negative) correlations imply that a model with an increase in the equator-to-pole surface temperature gradient shifts the metric further poleward. Correlations are plotted for the annual mean and the four seasonal means, and error bars denote the 95% confidence bounds on the correlation coefficients.

sensitivity, as they are not shared collectively across the CMIP5 ensemble, but their identification would be immensely challenging due to the fact that such mechanisms would be model specific.

6. Conclusions

Equilibrium climate sensitivity (ECS), the steady state global-mean surface temperature response to doubled atmospheric CO_2 concentrations, is sometimes viewed as an all-encompassing metric that describes the uncertainty in global climate models' responses to CO_2 forcing. Yet it is well known that, in enhanced CO_2 scenarios, the poleward boundary of the Hadley circulation ($\phi_{\Psi 500}$), the subtropical dry zones ($\phi_{P-E=0}$), and the midlatitude eddy-driven jets (ϕ_{u850}) shift poleward in global climate models (changes that we term

Table 3. Summary of the Statistically Significant Relationships Between ECS and Dynamical Sensitivity Found in This Paper[a]

	Southern Hemisphere	Northern Hemisphere
Midlatitude jet	Poleward shift Annual (20%) DJF (25%) MAM (36%)	Poleward shift in North Atlantic jet SON (42%) Equatorward shift in North Pacific jet JJA (52%)
Subtropical dry zone edge	Poleward shift Annual (44%) DJF (34%) MAM (56%)	
Hadley cell edge	Poleward shift Annual (59%) DJF (28%) MAM (64%) JJA (47%) SON (18%)	Poleward shift DJF (50%) Equatorward shift JJA (41%)

[a]The percentages in parentheses list the percentage of intermodel variance in each dynamical sensitivity metric explained by the intermodel variance in ECS.

dynamical sensitivity) and that these responses may be more important for societal impacts than the global-mean surface temperature response. In this study, we have asked if the intermodel spread in ECS in CMIP5 models can explain the intermodel spread in the dynamical sensitivity of the models. The statistically significant findings are summarized in Table 3.

For the SH, in particular, the dynamical sensitivity is strongly correlated with ECS. In the annual mean, intermodel differences in the value of ECS can explain as much as 59% of the spread in the SH Hadley cell expansion across models, 44% of the spread in the expansion of the SH subtropical dry zones, but only 20% of the spread in the SH midlatitude jet response (Table 3). The correlations are particularly robust during the DJF and MAM seasons (Figure 4a; see also GP14). During JJA and SON, the responses of SH ϕ_{u850} and SH $\phi_{P-E=0}$ to CO_2 forcing are more strongly linked to climatological biases in the models (GP14) and to the response of the equator-to-pole surface temperature gradient (Figure 10).

In contrast, for the NH, only a few aspects of dynamical sensitivity are correlated with ECS. In the annual mean, intermodel differences in the value of ECS can explain at best 7% of the spread in the Hadley cell expansion across models and provide virtually no information about the intermodel spread in the behavior of the subtropical dry zones or the zonal-mean midlatitude jet. Only the poleward expansion of $\phi_{\Psi 500}$ in DJF, the equatorward contraction of $\phi_{\Psi 500}$ in JJA, the poleward shift in North Atlantic ϕ_{u850} in SON, and the equatorward shift in North Pacific ϕ_{u850} in JJA are significantly correlated with ECS (Figures 4b and 9b and Table 3). In the NH, large residual components of dynamical sensitivity are found, which are unrelated to the intermodel spread in ECS: notably, the weakening of the NH branch of the Hadley circulation (Figure 5), the poleward expansion of the summertime tropical circulation (Figure 5c), and the poleward shifts in the midlatitude jets in all seasons but SON (Figures 8 and 9). The more complicated relationship between ECS and NH dynamical sensitivity likely reflects changes in climatological stationary waves, which are much stronger in the NH than in the SH [e.g., *Simpson et al.*, 2014].

Overall, the results here demonstrate that only some, but not all, of the intermodel spread in the atmospheric circulation response to CO_2 forcing in global climate models is linked to ECS. This is not surprising given that many of the mechanisms hypothesized to explain the atmospheric circulation's response to CO_2 forcing invoke the global-mean surface temperature, including increases in tropospheric static stability in the subtropics and midlatitudes and increases in the upper tropospheric-lower stratospheric equator-to-pole temperature gradient (Table 2). Yet other proposed mechanisms, particularly those linked to the direct radiative effects of CO_2, to changes in the stationary wave patterns, or to changes in the surface meridional temperature gradient, are not a function of the global-mean surface temperature but could, nonetheless, contribute nonnegligibly to the intermodel spread in the dynamical sensitivity of global climate models. Thus, while efforts to narrow the spread in ECS across global climate models focus on global-mean feedbacks, additional processes must be considered to narrow the spread in dynamical sensitivity across models.

Acknowledgments

We thank D.W.J. Thompson for the helpful discussions during the early stages of this project, and G. Vallis and two anonymous reviewers for their insightful reviews and comments. The ERA-Interim reanalysis data were obtained freely from the European Centre for Medium-Range Weather Forecasts (http://apps.ecmwf.int/datasets/). All model data used in this paper are freely available through the Earth System Grid Federation (https://pcmdi9.llnl.gov/projects/esgf-llnl/), as described in *Taylor et al.* [2012]. We acknowledge the World Climate Research Program's Working Group on Coupled Modelling, which is responsible for CMIP, and we thank the climate modeling groups (listed in Table 1) for producing and making available their model output. For CMIP, the U.S. Department of Energy's Program for Climate Model Diagnosis and Intercomparison provides coordinating support and led development of software infrastructure in partnership with the Global Organization for Earth System Science Portals. This material is based upon the work supported by the National Science Foundation under grant AGS-1522829. L.M.P. was supported by a National Science Foundation grant to Columbia University.

References

Arblaster, J. M., G. A. Meehl, and D. J. Karoly (2011), Future climate change in the Southern Hemisphere: Competing effects of ozone and greenhouse gases, *Geophys. Res. Lett.*, *38*, L02701, doi:10.1029/2010GL045384.

Barnes, E. A., and D. L. Hartmann (2010), Testing a theory for the effect of latitude on the persistence of eddy-driven jets using CMIP3 simulations, *Geophys. Res. Lett.*, *37*, L15801, doi:10.1029/2010GL044144.

Barnes, E. A., and L. M. Polvani (2013), Response of the midlatitude jets and of their variability to increased greenhouse gases in CMIP5 models, *J. Clim.*, *26*, 7117–7135.

Brayshaw, D. J., B. Hoskins, and M. Blackburn (2008), The storm-track response to idealized SST perturbations in an aquaplanet GCM, *J. Atmos. Sci.*, *65*, 2842–2860.

Butler, A. H., D. W. J. Thompson, and R. Heikes (2010), The steady-state atmospheric circulation response to climate change-like thermal forcings in a simple general circulation model, *J. Clim.*, *23*, 3474–3496.

Ceppi, P., Y.-T. Hwang, D. M. W. Frierson, and D. L. Hartmann (2012), Southern Hemisphere jet latitude biases in CMIP5 models linked to shortwave cloud forcing, *Geophys. Res. Lett.*, *39*, L19708, doi:10.1029/2012GL053115.

Ceppi, P., M. D. Zelinka, and D. L. Hartmann (2014), The response of the Southern Hemisphere eddy-driven jet to future changes in shortwave radiation in CMIP5, *Geophys. Res. Lett.*, *41*, 3244–3250, doi:10.1002/2014GL060043.

Chen, G., and I. M. Held (2007), Phase speed spectra and the recent poleward shift of Southern Hemisphere surface westerlies, *Geophys. Res. Lett.*, *34*, L21805, doi:10.1029/2007GL031200.

Chen, G., J. Lu, and D. M. W. Frierson (2008), Phase speed spectra and the latitude of surface westerlies: Interannual variability and global warming trend, *J. Clim.*, *21*, 5942–5959.

Chen, G., R. A. Plumb, and J. Lu (2010), Sensitivities of zonal mean atmospheric circulation to SST warming in an aqua-planet model, *Geophys. Res. Lett.*, *37*, L12701, doi:10.1029/2010GL043473.

Dee, D. P., et al. (2011), The ERA-Interim reanalysis: Configuration and performance of the data assimilation system, *Q. J. R. Meteorol. Soc.*, *137*, 553–597.

Deser, C., R. A. Tomas, and L. Sun (2015), The role of ocean–atmosphere coupling in the zonal-mean atmospheric response to Arctic sea ice loss, *J. Clim.*, *28*, 2168–2186.

Forster, P. M., T. Andrews, P. Good, J. M. Gregory, L. S. Jackson, and M. Zelinka (2013), Evaluating adjusted forcing and model spread for historical and future scenarios in the CMIP5 generation of climate models, *J. Geophys. Res. Atmos.*, *118*, 1139–1150.

Frierson, D. M. W., J. Lu, and G. Chen (2007), Width of the Hadley cell in simple and comprehensive general circulation models, *Geophys. Res. Lett.*, *34*, L18804, doi:10.1029/2007GL031115.

Gerber, E. P., and S.-W. Son (2014), Quantifying the summertime response of the austral jet stream and Hadley cell to stratospheric ozone and greenhouse gases, *J. Clim.*, *27*, 5538–5559.

Grise, K. M., and L. M. Polvani (2014a), Is climate sensitivity related to dynamical sensitivity? A Southern Hemisphere perspective, *Geophys. Res. Lett.*, *41*, 534–540, doi:10.1002/2013GL058466.

Grise, K. M., and L. M. Polvani (2014b), The response of mid-latitude jets to increased CO_2: Distinguishing the roles of sea surface temperature and direct radiative forcing, *Geophys. Res. Lett.*, *41*, 6863–6871, doi:10.1002/2014GL061638.

Harvey, B. J., L. C. Shaffrey, T. J. Woollings, G. Zappa, and K. I. Hodges (2012), How large are projected 21st century storm track changes?, *Geophys. Res. Lett.*, *39*, L18707, doi:10.1029/2012GL052873.

Harvey, B. J., L. C. Shaffrey, and T. J. Woollings (2014), Equator-to-pole temperature differences and the extra-tropical storm track responses of the CMIP5 climate models, *Clim. Dyn.*, *43*, 1171–1182.

Harvey, B. J., L. C. Shaffrey, and T. J. Woollings (2015), Deconstructing the climate change response of the Northern Hemisphere wintertime storm tracks, *Clim. Dyn.*, *45*, 2847–2860.

He, J., and B. J. Soden (2015), Anthropogenic weakening of the tropical circulation: The relative roles of direct CO_2 forcing and sea surface temperature change, *J. Clim.*, *28*, 8728–8742, doi:10.1175/JCLI-D-15-0205.1.

Held, I. M., and B. J. Soden (2006), Robust responses of the hydrological cycle to global warming, *J. Clim.*, *19*, 5686–5699.

Hu, Y., L. Tao, and J. Liu (2013), Poleward expansion of the Hadley circulation in CMIP5 simulations, *Adv. Atmos. Sci.*, *30*, 790–795.

Johanson, C. M., and Q. Fu (2009), Hadley cell widening: Model simulations versus observations, *J. Clim.*, *22*, 2713–2725.

Kang, S. M., and J. Lu (2012), Expansion of the Hadley cell under global warming: Winter versus summer, *J. Clim.*, *25*, 8387–8393.

Kang, S. M., and L. M. Polvani (2011), The interannual relationship between the latitude of the eddy-driven jet and the edge of the Hadley cell, *J. Clim.*, *24*, 563–568.

Kang, S. M., C. Deser, and L. M. Polvani (2013), Uncertainty in climate change projections of the Hadley circulation: The role of internal variability, *J. Clim.*, *26*, 7541–7554.

Kidston, J., and E. P. Gerber (2010), Intermodel variability of the poleward shift of the austral jet stream in the CMIP3 integrations linked to biases in 20th century climatology, *Geophys. Res. Lett.*, *37*, L09708, doi:10.1029/2010GL042873.

Kidston, J. S., S. M. Dean, J. A. Renwick, and G. K. Vallis (2010), A robust increase in eddy length scale in the simulation of future climates, *Geophys. Res. Lett.*, *37*, L03806, doi:10.1029/2009GL041615.

Kidston, J. S., G. K. Vallis, S. M. Dean, and J. A. Renwick (2011), Can the increase in the eddy length scale under global warming cause the poleward shift of the jet streams?, *J. Clim.*, *24*, 3764–3780.

Kushner, P. J., I. M. Held, and T. L. Delworth (2001), Southern Hemisphere atmospheric circulation response to global warming, *J. Clim.*, *14*, 2238–2249.

Lorenz, D. J. (2014), Understanding mid-latitude jet variability and change using Rossby wave chromatography: Poleward shifted jets in response to external forcing, *J. Atmos. Sci.*, *71*, 2370–2389.

Lorenz, D. J., and E. T. DeWeaver (2007), Tropopause height and zonal wind response to global warming in the IPCC scenario integrations, *J. Geophys. Res.*, *112*, D10119, doi:10.1029/2006JD008087.

Lu, J., G. A. Vecchi, and T. Reichler (2007), Expansion of the Hadley cell under global warming, *Geophys. Res. Lett.*, *34*, L06805, doi:10.1029/2006GL028443.

Lu, J., G. Chen, and D. M. W. Frierson (2008), Response of the zonal mean atmospheric circulation to El Niño versus global warming, *J. Clim.*, *21*, 5835–5851.

Lu, J., G. Chen, and D. M. W. Frierson (2010), The position of the midlatitude storm track and eddy-driven westerlies in aquaplanet ACGMS, *J. Atmos. Sci.*, *67*, 3984–4000.

Miller, R. L., G. A. Schmidt, and D. T. Shindell (2006), Forced annular variations in the 20th century Intergovernmental Panel on Climate Change Fourth Assessment Report models, *J. Geophys. Res.*, *111*, D18101, doi:10.1029/2005JD006323.

Polvani, L. M., and K. L. Smith (2013), Can natural variability explain observed Antarctic sea ice trends? New modeling evidence from CMIP5, *Geophys. Res. Lett.*, *40*, 3195–3199, doi:10.1002/grl.50578.

Ring, M. J., and R. A. Plumb (2008), The response of a simplified GCM to axisymmetric forcings: Applicability of the fluctuation-dissipation theorem, *J. Atmos. Sci.*, *65*, 3880–3898.

Santer, B. D., et al. (2003), Contributions of anthropogenic and natural forcing to recent tropopause height changes, *Science*, *301*, 479–483.

Scheff, J., and D. M. W. Frierson (2012), Robust future precipitation declines in CMIP5 largely reflect the poleward expansion of model subtropical dry zones. *Geophys. Res. Lett.*, *39*, L18704, doi:10.1029/2012GL052910.

Schneider, T., P. A. O'Gorman, and X. J. Levine (2010), Water vapor and the dynamics of climate changes, *Rev. Geophys.*, *48*, RG3001, doi:10.1029/2009RG000302.

Seager, R., N. Harnik, Y. Kushnir, W. Robinson, and J. Miller (2003), Mechanisms of hemispherically symmetric climate variability, *J. Clim.*, *16*, 2960–2978.

Seager, R., N. Naik, and G. A. Vecchi (2010), Thermodynamic and dynamic mechanisms for large-scale changes in the hydrological cycle in response to global warming, *J. Clim.*, *23*, 4651–4668.

Shaw, T. A., and A. Voigt (2015), Tug of war on summertime circulation between radiative forcing and sea surface warming, *Nat. Geosci.*, *8*, 560–566, doi:10.1038/ngeo2449.

Simpson, I., T. Shaw, and R. Seager (2014), A diagnosis of the seasonally and longitudinally varying mid-latitude circulation response to global warming, *J. Atmos. Sci.*, *71*, 2489–2515, doi:10.1175/JAS-D-13-0325.1.

Swart, N., and J. Fyfe (2012), Observed and simulated changes in the Southern Hemisphere surface westerly wind-stress, *Geophys. Res. Lett.*, *39*, L16711, doi:10.1029/2012GL052810.

Tandon, N. F., E. P. Gerber, A. H. Sobel, and L. M. Polvani (2013), Understanding Hadley cell expansion versus contraction: Insights from simplified models and implications for recent observations, *J. Clim.*, *26*, 4304–4321.

Taylor, K. E., R. J. Stouffer, and G. A. Meehl (2012), An overview of CMIP5 and the experiment design, *Bull. Am. Meteorol. Soc.*, *93*, 485–498.

Vallis, G. K., P. Zurita-Gotor, C. Cairns, and J. Kidston (2015), Response of the large-scale structure of the atmosphere to global warming, *Q. J. R. Meteorol. Soc.*, *141*, 1479–1501, doi:10.1002/qj.2456.

Vecchi, G. A., and B. J. Soden (2007), Global warming and the weakening of the tropical circulation, *J. Clim.*, *20*, 4316–4340.

Wilcox, L. J., A. J. Charlton-Perez, and L. J. Gray (2012), Trends in austral jet position in ensembles of high- and low-top CMIP5 models, *J. Geophys. Res.*, *117*, D13115, doi:10.1029/2012JD017597.

Yin, J. H. (2005), A consistent poleward shift of the storm tracks in simulations of 21st century climate, *Geophys. Res. Lett.*, *32*, L18701, doi:10.1029/2005GL023684.